UNITED NATIONS EDUCATIONAL, SCIENTIFIC AND CULTURAL ORGANIZATION
INTERNATIONAL CENTRE FOR THEORETICAL PHYSICS
I.C.T.P., P.O. BOX 586, 34100 TRIESTE, ITALY. CABLE: CENTRATOM TRIESTE

H4.SMR/449-6

WINTER COLLEGE ON HIGH RESOLUTION SPECTROSCOPY

(8 January - 2 February 1990)

COOPERATIVE FREQUENCY LOCKING AND STATIONARY SPATIAL STRUCTURES IN LASERS

L. A. LUGIATO, C. OLDANO

(**) L.M. NARDUCCI

Dipartimento di Fisica del Politecnico
10129 Torino, Italy

(**) Physics Department, Drexel University
Philadelphia, PA 19104, U.S.A.

Reprinted from Journal of the Optical Society of America B, Vol. 5, page 879, May 1988

Cooperative frequency locking and stationary spatial structures in lasers

L. A. Lugiato and C. Oldano

Dipartimento di Fisica del Politecnico, 10129 Torino, Italy

L. M. Narducci

Department of Physics, Drexel University, Philadelphia, Pennsylvania 19104

Received October 21, 1987; accepted January 14, 1988

We investigate the spontaneous emergence of transverse patterns in lasers by using both the standard two-level model and the so-called cubic approximation, which is generally valid in the threshold regions. The stationary intensity configurations fall into two distinct classes. The first includes solutions of the single-mode type with the frequency and spatial structure of one of the transverse resonances. The solutions of the second group involve the simultaneous oscillation of several cavity modes, operating in such a way as to produce a stationary intensity profile. The stationary character of these multimode configurations emerges from the fact that the transverse modes of the resonator lock onto a common frequency during the nonlinear transient. We call this phenomenon cooperative frequency locking.

1. INTRODUCTION

The spontaneous formation of stationary spatial structures in homogeneous systems has been the object of extensive investigations in such fields as nonlinear chemical reactions and developmental biology.[1-3] Here the instabilities that are responsible for the emergence of spatial patterns arise from a diffusive mechanism and are usually referred to as Turing instabilities.[4]

Optical systems are much more widely known for their propensity to produce temporal structures in the form of spontaneous oscillations of the regular or chaotic type.[5,6] Only recently has a Turing instability been discovered[7-10] in an optical model. Here, the resulting stationary pattern is produced by the interplay between diffraction and nonlinear coupling and not by a diffusion process. The optical arrangement found to produce these interesting new effects can be described as follows. A passive medium is contained in an optical ring or Fabry–Perot cavity fitted with an additional pair of lateral mirrors that act as a waveguide for the radiation field. With an appropriate selection of the state of polarization of the incident field, injected along the z direction, the electric field in the resonator acquires a uniform profile along the transverse y direction. The input field is uniform along the transverse direction, and its carrier frequency is almost resonant with the transition frequency of the intracavity medium and with one of the longitudinal modes.

Under normal conditions, the cavity and the output fields are also uniform in a plane transverse to the direction of propagation. When the input intensity exceeds a certain threshold level, diffraction may cause an instability that evolves, spontaneously, to a stationary spatial pattern along the x direction.

A typical condition for the emergence of this instability is that the frequency spacing between the resonant longitudinal mode and the nearest transverse resonances be of the order of the cavity linewidth. This situation creates a competition between transverse and longitudinal modes. The end result is the loss of stability of the spatially homogeneous stationary solution. At the same time the input field imposes its oscillation frequency on the competing modes, so that the eventual stationary state displays no temporal intensity modulation.

Our aim in this paper is twofold. First, we extend the description of the spatial pattern formation to the case of an active system, such as a homogeneously broadened laser with detuning between the atomic transition frequency and the longitudinal cavity modes. Second, we show that in the case of the laser the occurrence of the spatial patterns is accompanied by a new phenomenon, which we propose to call cooperative frequency locking.

The novelty here resides in the fact that a typical laser system operates either in a single or in a multimode configuration and that in the multimode case the output intensity undergoes oscillations caused by the interference among the competing modes. The stationary spatial structure described in this paper corresponds to a different type of multimode operation in which the coexisting modes select, cooperatively, a common operating frequency and enter a regime of synchronous oscillation at the end of the transient evolution. The absence of beat notes produces a stationary output pattern instead of the more familiar pulsations.

In Section 2 we describe the details of the geometrical configuration of our model. The mathematical description of this system is given in Section 3 for the case of a ring cavity and in Section 4 for a Fabry–Perot configuration. In Section 5 we reformulate the time-evolution equations in terms of modal amplitudes. In Section 6 we carry out a linear-stability analysis and identify the domains of instability. Section 7 contains a classification of the different stationary-intensity solutions. Section 8 illustrates the results of

0740-3224/88/050879-10$02.00

the numerical integration of the modal equations of motion. An overview of our predictions and some concluding comments are presented in Section 9.

2. DESCRIPTION OF THE CAVITY

We consider a cavity defined by four mirrors with transmittance coefficient $T \ll 1$. Two mirrors are orthogonal to the longitudinal z axis and are positioned at a distance L; the other two are orthogonal to the x axis and at a distance b from one another (see Fig. 1). The cavity is open along the y direction and contains a homogeneously broadened medium, which is pumped into a state of inversion, as required for laser action. We fix the geometrical arrangement in such a way that the inequality

$$L \gg b \tag{2.1}$$

is satisfied. This ensures maximum gain along the z axis, which also becomes the direction of emission of the laser radiation. This requirement must be balanced by the assumption that the Fresnel number,

$$\mathcal{F} = \frac{b^2}{\lambda L}, \tag{2.2}$$

is sufficiently large to maintain the parameter

$$a = \frac{1}{2\pi\mathcal{F}T} \tag{2.3}$$

of the order of unity (or smaller), even if $T \ll 1$; λ, as usual, denotes the wavelength of the laser light.

We assume that the magnetic-field component of the cavity field is parallel to the y axis so that both the electric and magnetic fields become independent of the variable y. If the walls of the resonator are made of a conducting material, the cavity modes have the structure

$$E_x \propto \cos(k_x x)\sin(k_z z), \tag{2.4a}$$

$$E_z \propto \sin(k_x x)\cos(k_z z), \tag{2.4b}$$

$$H_y \propto \cos(k_x x)\cos(k_z z), \tag{2.4c}$$

where

$$k_x = \frac{\pi n}{b}, \qquad k_z = \frac{\pi n_z}{L}, \tag{2.5}$$

and n and n_z are nonnegative integer numbers. In particular, the choice $n = 0$ corresponds to the set of longitudinal modes of the resonator.

Our analysis is based on the paraxial approximation

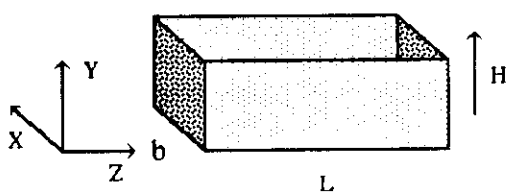

Fig. 1. Schematic representation of the Fabry–Perot cavity configuration discussed in this paper. The four mirrors have a transmittance coefficient $T \ll 1$. The cavity is open in the y direction, which is also the direction of the magnetic field H.

$$k_x \ll k_z. \tag{2.6}$$

In addition, because the transversality condition requires that

$$E_z/E_x \propto k_x/k_z,$$

we will neglect the small component E_z in view of expression (2.6). It follows that the electric field is essentially polarized along the x direction and is given by a superposition of modal functions of the type

$$\cos\left(\frac{\pi}{b}nx\right)\sin\left(\frac{\pi}{L}n_z z\right). \tag{2.7}$$

Reference 10 describes in detail the ring version of this cavity, whose modal functions have the structure

$$\cos\left(\frac{\pi}{b}nx\right)\exp\left(i\frac{2\pi}{L}n_z z\right), \tag{2.8}$$

where L still denotes the length of the resonator, and the parameter a that appears in Eq. (2.3) is now defined as

$$a = \frac{1}{4\pi\mathcal{F}T}. \tag{2.9}$$

For both Fabry–Perot and ring configurations we assume that the initial parameters were selected in such a way that the atomic line is in exact resonance with the longitudinal cavity mode, corresponding to a selected integer $n_z = m_z$. In this case the laser above threshold approaches a stationary state, and the field oscillates with the frequency of the m_z mode. At this point we detune the laser away from resonance and look for instabilities of the stationary state.

3. THE RING RESONATOR MODEL

We describe the medium as a collection of homogeneously broadened two-level atoms with transition frequency ω_A. We denote by $\gamma_\perp$ and $\gamma_\parallel$ the relaxation rates of the atomic polarization and population difference, respectively, and with σ the inversion per atom induced by the pump.

We consider first the simpler case of a ring cavity. The derivation of our model from the Maxwell–Bloch equations in the paraxial approximation is described in detail in Ref. 10. We introduce two main approximations:

(a) The uniform field limit, defined by the conditions

$$\alpha L \ll 1, \qquad T \ll 1, \tag{3.1}$$

with

$$C \equiv \frac{\alpha L \sigma}{2T} \tag{3.2}$$

arbitrary, where α is the gain coefficient of the electric field per unit length and C is the pump parameter. Note that the adjective uniform refers only to the longitudinal direction.

(b) The limit

$$\frac{\gamma_\perp L}{2\pi c} \ll 1, \tag{3.3}$$

which ensures laser operation in a single longitudinal mode. To be more precise, condition (3.3) selects the longitudinal mode $n_z = m_z$, which is the closest to the atomic line center. Note that the transverse modal index n, instead, remains

free to vary over the range 0, 1, 2, ... so that our model accounts for the evolution of an infinite number of transverse modes.

As a consequence of approximations (a) and (b), the electric field has the structure

$$E_x = E(x,t)\exp\left(i\frac{2\pi}{L}m_z z\right)\exp(-i\omega_R t) + \text{c.c.}, \tag{3.4}$$

where ω_R is a reference frequency that can be chosen arbitrarily. As a consequence of Eq. (2.8) the field envelope can be represented as the linear combination of modal functions according to

$$E(x,t) = \sum_{n=0}^{\infty} f_n(t)\cos(\pi n x'), \tag{3.5}$$

where f_n denotes the nth modal amplitude and the scaled space variable is defined by

$$x' = x/b. \tag{3.6}$$

With this choice we see that the envelope E obeys the reflectivity boundary condition, $\partial E/\partial x' = 0$, on the lateral mirrors at $x' = 0$ and $x' = 1$.

The space-time-dependent equations have the form[10]

$$\frac{\partial E}{\partial t} = -\kappa\left[(1+i\theta)E - 2CP - ia\frac{\partial^2 E}{\partial x'^2}\right], \tag{3.7}$$

$$\frac{\partial P}{\partial t} = -\gamma_\perp[(1+i\Delta)P - ED], \tag{3.8}$$

$$\frac{\partial D}{\partial t} = -\gamma_\parallel[D - 1 + \tfrac{1}{2}(E^*P + EP^*)], \tag{3.9}$$

where the normalized variables P and D describe the atomic polarization and population inversion, respectively. The variables E^* and P^* obey the complex-conjugate equations (3.7) and (3.8). The cavity damping constant, or cavity linewidth, κ, is defined as

$$\kappa = \frac{cT}{L}. \tag{3.10}$$

The cavity detuning parameter, θ, and the atomic detuning parameter, Δ, are given by

$$\theta = \frac{\omega_C - \omega_R}{\kappa}, \qquad \Delta = \frac{\omega_A - \omega_R}{\gamma_\perp}, \tag{3.11}$$

where $\omega_C = 2\pi c m_z/L$ is the frequency of the resonant longitudinal mode. The variables E, P, and D depend on both the time and the scaled space variable x'; the term $\partial^2 E/\partial x'^2$ corresponds to the transverse Laplacian after taking into account that E is independent of y.

In what follows we choose the reference frequency ω_R as the laser carrier frequency in the single-mode regime of operation corresponding to $n_z = m_z$ and $n = 0$. Thus ω_R is given by the mode-pulling formula

$$\omega_R = \frac{\kappa\omega_A + \gamma_\perp\omega_C}{\kappa + \gamma_\perp}, \tag{3.12}$$

which is equivalent to the relation

$$\Delta = -\theta, \tag{3.13}$$

which we can verify at once by using Eqs. (3.11). In fact, the time- and space-independent solutions of Eqs. (3.7)–(3.9) lead to Eq. (3.13) and to the results

$$|E|^2 = 2C - 1 - \theta^2, \qquad P = \frac{1+i\theta}{2C}E, \qquad D = \frac{1+\theta^2}{2C}, \tag{3.14}$$

with an arbitrary phase for E. Equations (3.14) give the *transversally homogeneous* stationary solution of our problem.

In the good-cavity limit

$$\kappa \ll \gamma_\perp, \gamma_\parallel \tag{3.15}$$

we can eliminate the atomic variables adiabatically by setting $\partial D/\partial t = \partial P/\partial t = 0$ in Eqs. (3.8) and (3.9) and obtain the field evolution equation

$$\kappa^{-1}\frac{\partial E}{\partial t} = -E(1+i\theta)\left(1 - \frac{2C}{1+\theta^2+|E|^2}\right) + ia\frac{\partial^2 E}{\partial x'^2}. \tag{3.16}$$

In the threshold region, where $|E|^2$ is much smaller than the quantity $1+\theta^2$, we can introduce the approximation

$$\frac{1}{1+\theta^2+|E|^2} \cong \frac{1}{1+\theta^2} - \frac{|E|^2}{(1+\theta^2)^2}, \tag{3.17}$$

so that after

$$\mathcal{E} = \frac{(2C)^{1/2}}{1+\theta^2}E,$$

$$r = \frac{2C}{1+\theta^2} - 1 \tag{3.18}$$

are defined, the approximate form of the field equation becomes

$$\kappa^{-1}\frac{\partial \mathcal{E}}{\partial t} = -\mathcal{E}(1+i\theta)(|\mathcal{E}|^2 - r) + ia\frac{\partial^2 \mathcal{E}}{\partial x'^2}. \tag{3.19}$$

This equation supports the spatially homogeneous stationary solution

$$|\mathcal{E}|^2 = r. \tag{3.20}$$

Above threshold, i.e., for $r > 0$, the number of independent parameters in Eq. (3.19) can be reduced by defining the scaled quantities

$$\tau = \kappa r t,$$

$$E' = \mathcal{E}/r^{1/2},$$

$$a' = a/r, \tag{3.21}$$

so that Eq. (3.19) acquires the final form

$$\frac{\partial E'}{\partial \tau} = -E'(1+i\theta)(|E'|^2 - 1) + ia'\frac{\partial^2 E'}{\partial x'^2}. \tag{3.22}$$

The variable E'^*, of course, obeys the complex conjugate of Eq. (3.22).

4. FABRY-PEROT RESONATOR MODEL

In the case of a Fabry–Perot cavity, we must replace Eqs. (3.4) and (3.7)–(3.9) with[10]

$$E_x = E(x,t)\cos\left(\frac{\pi}{L}m_z z\right)\exp(-i\omega_0 t) + \text{c.c.} \tag{4.1}$$

and

$$\frac{\partial E}{\partial t} = -\kappa\left[(1+i\theta)E - 2C \times \int_{-\pi}^{+\pi} d\eta \cos\eta\, P(x',\eta,t) - ia\frac{\partial^2 E}{\partial x'^2}\right], \tag{4.2}$$

$$\frac{\partial P}{\partial t} = -\gamma_\perp[(1+i\Delta)P - 2ED\cos\eta], \tag{4.3}$$

$$\frac{\partial D}{\partial t} = -\gamma_\parallel[D - 1 + (E^*P + EP^*)\cos\eta], \tag{4.4}$$

where the variable η takes into account the standing-wave structure of the field inside the resonator. The parameter a is defined as in Eq. (2.3); the quantities κ and C are given by

$$\kappa = \frac{cT}{2L}, \qquad C = \frac{\alpha L\sigma}{T} \tag{4.5}$$

instead of Eqs. (3.10) and (3.2), respectively.

Also in the case of the Fabry–Perot geometry we can introduce the good-cavity limit (3.15) and a threshold region approximation similar to Eq. (3.17). The result is given again by Eq. (3.19), as we can easily verify with appropriate redefinitions of the parameter r and of the proportionality constant that links $\mathcal{E}$ to E'. In fact Eqs. (3.19) and (3.22) are valid in the threshold region for both ring and Fabry–Perot cavities and for homogeneously and inhomogeneously broadened active media.

5. MODAL AMPLITUDE EQUATIONS

It is convenient to reformulate the basic equations of our model in terms of the modal amplitudes f_n, p_n, and d_n defined by Eq. (3.5) and by the corresponding expansions

$$P(x',t) = \sum_{n=0}^{\infty} p_n(t)\cos(\pi n x'), \tag{5.1a}$$

$$D(x',t) = \sum_{n=0}^{\infty} d_n(t)\cos(\pi n x'). \tag{5.1b}$$

In this connection it may be useful to stress that the set of functions $\{\cos, \pi n x'\}$, $n = 0, 1, \ldots$ is complete over the interval (0, 1) and obeys the orthogonality relation

$$\int_0^1 dx' \cos(\pi n x')\cos(\pi m x') = \tfrac{1}{2}(\delta_{n,0}\delta_{m,0} + \delta_{n,m}). \tag{5.2}$$

In what follows we analyze in detail only the ring-cavity model [Eqs. (3.7)–(3.9)] and the universal cubic limit described by Eq. (3.22). On inserting Eqs. (3.5) and (5.1) into Eqs. (3.7)–(3.9) and taking Eq. (5.2) into account, we obtain the following set of equations for the modal amplitudes:

$$\frac{df_n}{dt} = -\kappa[(1+i\theta)f_n - 2Cp_n + ia(n)f_n], \tag{5.3}$$

$$\frac{dp_n}{dt} = -\gamma_\perp\left[(1-i\theta)p_n - \frac{1}{2(1+\delta_{n,0})}\sum_m \sum_{1\geq 0}^{*} f_m d_l\right], \tag{5.4}$$

$$\frac{dd_n}{dt} = -\gamma_\parallel\left[d_n - \delta_{n,0} + \frac{1}{4(1+\delta_{n,0})} \times \sum_m \sum_{1\geq 0}^{*} (f_m p_l^* + f_m^* p_l)\right], \tag{5.5}$$

where we have defined

$$a(n) = a\pi^2 n^2 \tag{5.6}$$

and where the asterisk applied to the summation sign indicates that the sum is restricted to the terms $1 = n + m$, $1 = n - m$, $1 = m - n$, and $1 = -m - n$, provided that $1 \geq 0$. The spatially homogeneous stationary solution (3.14) corresponds to the amplitudes

$$|f_n|^2 = (2C - 1 - \theta^2)\delta_{n,0},$$
$$p_n = \frac{1+i\theta}{2C} f_n,$$
$$d_n = \frac{1+\theta^2}{2C}\delta_{n,0}, \tag{5.7}$$

with an arbitrary phase for f_0. If we ignore all amplitudes in Eqs. (5.3)–(5.5) except those labeled by $n = 0$, the resulting set of equations reduces to the well-known single-mode Lorenz–Haken model.[11]

In a similar way, if we introduce the expansion

$$E'(x',t) = \sum_{n=0}^{\infty} f_n(t)\cos(\pi n x') \tag{5.8}$$

into Eq. (3.22), the corresponding set of modal equations becomes

$$\frac{df_n}{d\tau} = (1+i\theta)\left[f_n - \frac{1}{4(1+\delta_{n,0})}\sum_m \sum_l \sum_{s\geq 0}^{*} f_m f_l f_s^*\right] - ia'(n)f_n, \tag{5.9}$$

where we have introduced the notation

$$a'(n) = a'\pi^2 n^2 \tag{5.10}$$

and where the asterisk implies that the sum is restricted to terms with positive s and with $s = \pm n \pm m \pm 1$. Note that all combinations of upper and lower signs must be included.

The spatially homogeneous stationary solution (3.20) corresponds to the amplitudes

$$|f_n|^2 = \delta_{n,0}, \tag{5.11}$$

with an arbitrary phase for f_0. The parameter $a(n)$ defined by Eq. (5.6) represents the frequency spacing between the nth transverse resonance and the longitudinal mode $n = 0$, as measured in units of the cavity linewidth κ. In fact, for $k_x \ll k_z$ we have

$$\omega_n = c(k_x^2 + k_z^2)^{1/2} \cong \omega_0 + c\frac{k_x^2}{2k_z}, \tag{5.12}$$

where

$$\omega_0 = \omega_C = ck_z = 2\pi c m_z/L.$$

On taking into account that $k_x = \pi n/b$, $k_z = 2\pi/\lambda$, and Eqs. (3.10), (2.2) and (2.9), we find that

$$\frac{\omega_n - \omega_0}{\kappa} = a\pi^2 n^2 = a(n). \tag{5.13}$$

6. LINEAR-STABILITY ANALYSIS

We investigate now the stability of the homogeneous stationary solution against the growth of transverse modes with $n \neq 0$. For this purpose we introduce the fluctuation variables δf_n, δp_n, and δd_n, describing the deviations of the corresponding modal amplitudes from their stationary values (5.7), and we linearize Eqs. (5.3)–(5.5) with respect to these fluctuations.

A remarkable feature of the linearized equations is that the fluctuation variables δf_n, δf_n^*, δp_n, δp_n^*, and δd_n obey a self-contained set of equations for all values of the index n. These equations are given by

$$\frac{d\delta f_n}{dt} = -\kappa[(1 + i\theta)\delta f_n - 2C\,\delta p_n + ia(n)\delta f_n], \tag{6.1}$$

$$\frac{d\delta p_n}{dt} = -\gamma_\perp\left[(1 - i\theta)\delta p_n - f_0\delta d_n - \frac{1 + \theta^2}{2C}\,\delta f_n\right], \tag{6.2}$$

$$\frac{d\delta d_n}{dt} = -\gamma_\parallel\left(\delta d_n + \tfrac{1}{2}f_0\left\{\delta p_n + \delta p_n^* + \frac{1}{2C}\left[(1 + i\theta)\delta f_n^* + (1 - i\theta)\delta f_n\right]\right\}\right), \tag{6.3}$$

where we used Eqs. (5.7) and set

$$f_0 = (2C - 1 - \theta^2)^{1/2}, \tag{6.4}$$

fixing, in the process, the arbitrary phase of the steady-state field. (Note, however, that the following results are independent of this choice.) The variables δf_n^*, and δp_n^* obey the complex-conjugate equations (6.1) and (6.2). The ansatz

$$\begin{bmatrix} \delta f_n(t) \\ \delta f_n^*(t) \\ \delta p_n(t) \\ \delta p_n^*(t) \\ \delta d_n(t) \end{bmatrix} = e^{\lambda t} \begin{bmatrix} b_n \\ c_n \\ u_n \\ v_n \\ w_n \end{bmatrix} \tag{6.5}$$

leads to a linear, homogeneous, algebraic set of equations for b_n, c_n, u_n, v_n, and w_n, which admits nontrivial solutions when λ obeys the eigenvalue equation

$$\lambda^5 + a_4^{(n)}\lambda^4 + a_3^{(n)}\lambda^3 + a_2^{(n)}\lambda^2 + a_1^{(n)}\lambda + a_0^{(n)} = 0. \tag{6.6}$$

The explicit expressions of the coefficients $a_i^{(n)}$ ($i = 0, 1, \ldots 4$) are reported in Appendix A. For $n = 0$, the characteristic equation [Eq. (6.6)] reduces to that of the Lorenz–Haken model with detuning.[12] As a result, our model predicts the Lorenz–Haken instability, as a special case, which is well known to yield temporal oscillations. Here we put our emphasis on instabilities that produce stationary spatial structures; these are identified by the condition[10] $a_0^{(n)} \leq 0$. On the basis of Eq. (A5) of Appendix A, this condition takes the form

$$a(n) \leq -\frac{2\theta f_0^2}{1 + \theta^2 + f_0^2} = -\frac{\theta}{C}(2C - 1 - \theta^2). \tag{6.7}$$

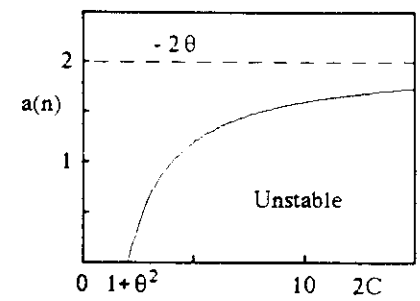

Fig. 2. Ring-cavity configuration. Domain of instability in the plane of the variables $a(n) = a\pi^2n^2$ and C for $\theta = -1$.

Hence the instability of interest to this work requires the validity of the following two conditions:

(a) θ must be negative or, equivalently, Δ must be positive [see Eq. (3.13)];

(b) At least one of the numbers $a(n) = a\pi^2n^2$ for $n = 1, 2, \ldots$ must satisfy Eq. (6.7).

The values of n such that $a(n)$ obeys inequality (6.7) identify the transverse modes that become unstable.

Figure 2 shows the instability domain in the plane of the variables $a(n)$ and C for $\theta = -1$. Note that this instability arises in the vicinity of the threshold $C_{thr} = (1 + \theta^2)/2$ when $a(1) = a\pi^2$ is small. For $C \to \infty$, the boundary of the instability domain defined by Eq. (6.7) has an asymptote for $a(n) = -2\theta$. In terms of the definition of θ and $a(n)$ in Eqs. (3.11) and (5.13), the condition $a(n) < -2\theta$ can be restated as

$$\omega_n - \omega_R < \omega_R - \omega_0. \tag{6.8}$$

In a similar way we can work out the stability analysis of the homogeneous stationary solution (5.11) of the universal cubic model (5.9). The result is the quadratic eigenvalue equation

$$\lambda^2 + 2\lambda + a'(n)[a'(n) + 2\theta] = 0, \tag{6.9}$$

leading to the instability condition

$$a'(n) \leq -2\theta \quad \text{or} \quad a(n) \leq -2\theta r. \tag{6.10}$$

With the help of Eqs. (3.18), we can verify immediately that expressions (6.10) coincide with the first-order approximation of Eq. (6.7) for $r \ll 1$.

7. NONUNIFORM STATIONARY-INTENSITY SOLUTION

In the unstable region defined by Eq. (6.7) [or Eq. (6.10)] we search for other stationary-intensity solutions of the form

$$E(x', t) = \exp(-i\delta\kappa t)E_s(x'), \tag{7.1a}$$

$$P(x', t) = \exp(-i\delta\kappa t)P_s(x'), \tag{7.1b}$$

$$D(x', t) = D_s(x'). \tag{7.1c}$$

When Eqs. (7.1) are substituted into Eqs. (3.7)–(3.9), the field equation becomes

$$i\delta E_s = (1 + i\theta)E_s - 2CP_s - ia\frac{\partial^2 E_s}{\partial x'^2}, \tag{7.2}$$

while the atomic equations yield

$$P_s = E_s \frac{1 + i(\theta + \delta\kappa')}{1 + (\theta + \delta\kappa')^2 + |E_s|^2}, \tag{7.3a}$$

$$D_s = \frac{1 + (\theta + \delta\kappa')^2}{1 + (\theta + \delta\kappa')^2 + |E_s|^2}, \tag{7.3b}$$

where

$$\kappa' = \kappa/\gamma_\perp. \tag{7.3c}$$

By inserting Eq. (7.3a) into Eq. (7.2) and on multiplication by E_s^*, we obtain

$$i\delta |E_s|^2 = (1 + \theta)|E_s|^2 - 2C|E_s|^2 \times \frac{1 + i(\theta + \delta\kappa')}{1 + (\theta + \delta\kappa')^2 + |E_s|^2} - ia \frac{\partial^2 E_s}{\partial x'^2} E_s^*. \tag{7.4}$$

Adding and subtracting Eq. (7.4) and its complex conjugate yields

$$0 = |E_s|^2 \left[1 - \frac{2C}{1 + (\theta + \delta\kappa')^2 + |E_s|^2}\right] + i \frac{a}{2} \frac{\partial}{\partial x'} \times \left(E_s \frac{\partial E_s^*}{\partial x'} - E_s^* \frac{\partial E_s}{\partial x'}\right). \tag{7.5}$$

$$0 = |E_s|^2 \left[\theta - \delta - \frac{2C(\theta + \delta\kappa')}{1 + (\theta - \delta\kappa')^2 + |E_s|^2}\right] - \frac{a}{2} \frac{\partial}{\partial x'} \times \left(E_s \frac{\partial E_s^*}{\partial x'} + E_s^* \frac{\partial E_s}{\partial x'}\right) + a \left|\frac{\partial E_s}{\partial x'}\right|^2. \tag{7.6}$$

Next we integrate over the variable x' in the range $(0, 1)$ and take into account the boundary conditions. If we denote the integral operation with angle brackets, the result can be expressed in the form

$$\langle |E_s|^2 \rangle = 2C \left\langle \frac{|E_s|^2}{1 + (\theta + \delta\kappa')^2 + |E_s|^2} \right\rangle. \tag{7.7}$$

$$\langle |E_s|^2 \rangle (\theta - \delta) = 2C (\theta + \delta\kappa') \left\langle \frac{|E_s|^2}{1 + (\theta + \delta\kappa')^2 + |E_s|^2} \right\rangle - a \left\langle \left|\frac{\partial E_s}{\partial x'}\right|^2 \right\rangle. \tag{7.8}$$

On substituting Eq. (7.7) into Eq. (7.8), we obtain

$$\delta = \frac{a}{1 + \kappa'} \frac{\left\langle \left|\frac{\partial E_s}{\partial x'}\right|^2 \right\rangle}{\langle |E_s|^2 \rangle}. \tag{7.9}$$

In terms of the modal expansion

$$E_s(x') = \sum_{n=0}^{\infty} f_n \cos(\pi n x'), \tag{7.10}$$

and with the help of Eqs. (5.2) and (5.6), we can recast Eq. (7.9) in the more useful form

$$\delta = \frac{1}{1 + \kappa'} \frac{\sum_{n=1}^{\infty} |f_n|^2 a(n)}{2|f_0|^2 + \sum_{n=1}^{\infty} |f_n|^2}, \tag{7.11}$$

which expresses the frequency δ as an average of the parameters $a(n)$ weighted over the distribution $|f_n|^2$. Note that the stationary-intensity solutions depend on κ' by way of δ, whereas in the case of passive systems they do not depend on the cavity linewidth.[7-10]

If instead of using Eqs. (3.7)–(3.9) we begin from the cubic model (3.22) and follow the same procedure, we arrive at the same result [Eq. (7.11)] but without the factor $(1 + \kappa')^{-1}$. Furthermore, Eq. (7.7) is replaced by the simpler-looking relation

$$\langle |E_s|^2 \rangle = \langle |E_s|^4 \rangle. \tag{7.12}$$

On the basis of Eqs. (5.3)–(5.5) or Eq. (5.9), the stationary-intensity solutions can be classified into two distinct groups.

(a) Let $k \geq 0$ be an arbitrary integer. The first group of solutions is characterized by modal amplitudes f_n and p_n, which are different from zero only for $n = (2s + 1)k$, with $s = 0, 1, 2, \ldots$, and d_n is different from zero for $n = 2sk$.

(b) Let $k > 0$ be an arbitrary integer. The second group of solutions is characterized by modal amplitudes f_n, p_n and d_n, which are different from zero only for $n = sk$, with $s = 0, 1, 2, \ldots$. The modal amplitudes p_n and d_n, of course, are defined by the expansions

$$P_s(x') = \sum_{n=0}^{\infty} p_n \cos(\pi n x'), \tag{7.13a}$$

$$D_s(x') = \sum_{n=0}^{\infty} d_n \cos(\pi n x'). \tag{7.13b}$$

Note that a special case of the solutions of type (a) for $k = 0$ is the spatially homogeneous stationary solution for which only the components f_0, p_0, and d_0 are nonvanishing, and $\delta = 0$. The other solutions of type (a) corresponding to $k > 0$ have the amplitude f_k and its odd harmonics as their only nonvanishing field components. Our numerical results show that the harmonic components are actually quite small; thus these types of solution are essentially of the single-mode type and have the spatial structure of the kth transverse mode.

If we neglect all amplitudes except for f_k, p_k, d_0, and d_{2k} in Eqs. (5.3)–(5.5), we obtain the following approximate expression for the amplitudes of the single-mode solutions

$$|f_k|^2 = \frac{4}{3}\{2C - [1 + (\theta + \delta\kappa')^2]\}, \tag{7.14}$$

with

$$\delta = \frac{a(k)}{1 + \kappa'}. \tag{7.15}$$

Note that Eq. (7.15) agrees with the general relation of Eq. (7.11) and that in terms of Eqs. (3.12) and (5.13) the oscillation frequency, in this case, is given by

$$\omega_k' = \omega_R + \delta\kappa = \frac{\kappa\omega_A + \gamma_\perp\omega_k}{\kappa + \gamma_\perp}, \tag{7.16}$$

which is again the usual mode-pulling formula. In the case of the cubic equation, instead, we obtain

$$|f_k|^2 = \frac{4}{3} \quad \text{and} \quad \delta = a(k) \tag{7.17}$$

in place of Eqs. (7.14) and (7.15), respectively.

The existence of the single-mode solutions for $k \neq 0$ extends to the transverse modes a property that is already known from the plane-wave theory: as shown, for example, in Ref. 13, an infinite number of stationary solutions can be found, each corresponding to a different longitudinal mode. The modes are defined for an empty cavity, so that the existence of single-mode stationary solutions in the presence of an active medium is certainly a nontrivial result. As it turns out, under uniform field conditions, the nonlinearity induced by the medium produces only a small admixture of the odd harmonics of the fundamental mode.

The solutions of type (a) for $k \neq 0$ are indeed inhomogeneous stationary solutions that emerge when the laser undergoes a transition from the longitudinal mode $k = 0$ into another modal configuration corresponding to a different value of k. However, these solutions are not especially interesting from the viewpoint of spatial pattern formation. Much more intriguing, instead, are the solutions of type (b) in which the longitudinal mode $n = 0$ coexists with a number of other transverse modes of comparable strength. As in the case of the stationary solutions of Refs. 7–10, here also we have the formation of potentially complicated and interesting spatial patterns.

An additional important feature of solutions of this class is that they represent a new type of operation for the laser. In fact, from traditional laser theory we recognize two types of behavior:

(i) Single-mode operation, in which one mode suppresses all the others.

(ii) Multimode operation, in which different modes coexist and compete with one another.

In the usual multimode behavior each mode oscillates with a different frequency; thus the total electric field takes the form

$$\sum_n f_n g_n(\mathbf{x}')\exp(-i\omega_n' t) + \text{c.c.}, \tag{7.18}$$

where ω_n' is the mode-pulled frequency of the nth mode and the factor $g_n(\mathbf{x}')$ describes its spatial structure. In this case the field intensity acquires a time dependence because of the interference of the modes with one another.[14] In our case, instead, Eqs. (3.4) and (7.1) lead to a field structure of the form

$$E_x = \sum_n f_n \cos(\pi n x')\exp(i\frac{2\pi}{L} m_z z) \times \exp[-i(\omega_R + \delta\kappa)t] + \text{c.c.} \tag{7.19}$$

so that the intensity is stationary in time. In this type of operation the modes do compete with one another, but, in the course of the nonlinear evolution, they acquire and maintain a common frequency of oscillation. For this reason we call this new phenomenon cooperative frequency locking. This behavior eliminates the beat notes, or perhaps one can even say that the modes beat against one another in space and not in time. According to Eq. (7.11) the common oscillation frequency falls within the range spanned by the mode-pulled frequencies of the coexisting modes.

8. NUMERICAL RESULTS

We consider the ring-cavity model of Eqs. (3.7)–(3.9) and the corresponding eigenvalue equation (6.6). With the help of the Routh–Hurwitz criterion[2] applied to Eq. (6.6), we can construct the instability domain in the plane of the variables $a(1)$ and f_0^2. A few examples are shown in Fig. 3 for $\kappa' = 0.1$, $\gamma_\parallel/\gamma_\perp = 1$, and a few values of θ. Depending on the selection of the parameters, we can have two or even three domains of instability. The lower domain [in relation to the vertical $a(1)$ axis] is defined by the condition $a_0^{(n)} < 0$, i.e., by inequality (6.7); the upper domains originate from the remaining conditions of the Routh–Hurwitz criterion. In Fig. 3(d) we note the coalescence of the two upper instability domains, which are still distinct in Fig. 3(c). This feature is common also to other parameter values.

We have solved the nonlinear time-dependent modal equations (5.3)–(5.5) with a fourth-order Runge–Kutta algorithm; in our simulations we have used, typically, a maximum modal index $n_{\max} = 15$ and performed frequent checks of convergence with a larger number of modal amplitudes. A typical scan proceeds by selecting θ, κ', $\gamma_\parallel/\gamma_\perp$, and f_0^2 [this fixes the value of the gain parameter C by way of Eq. (6.4)] and by varying the parameter $a(1) = a\pi^2$. Each run begins with an initial condition corresponding to the spatially homogeneous solution (5.7), perturbed by a small amount of Gaussian random noise.

In this paper we consider only those cases in which the unstable modes fall inside the lower instability domain, such as we have for $\kappa' = 0.1$, $\gamma_\parallel/\gamma_\perp = 1$, $\theta = -0.6$, and $f_0^2 = 2$ (see Fig. 3). The result of the scans can be summarized as shown qualitatively in Fig. 4. Depending of the value of $a(1)$, we can divide the lower instability domain into three zones, labeled A, B, and C for convenience. Values of $a(1)$ in zone A lead to stationary single-mode solutions, in excellent agreement with the analytic formulas (7.14) and (7.15). Values of $a(1)$ in regions B and C lead to multimode stationary solutions with cooperative frequency locking. Region C corresponds to values of $a(1)$ such that not only mode $n = 1$ but also $n = 2$ is unstable.

We now consider the case $\kappa' = 0.1$, $\gamma_\parallel/\gamma_\perp = 1$, $\theta = -0.6$, and $f_0^2 = 2$ in some detail. The value $a(1) = 0.65$ lies in region A; the mode $n = 1$ builds up initially, and the system appears to approach a multimode stationary solution, which, however, turns out to be unstable in this case. As a result, the system eventually develops a single-mode structure of type (a) with $k = 2$, as described in Section 7. The values of $|f_n|^2$ for the odd harmonics of $n = 2$ are smaller than $|f_2|^2$ by at least 3 orders of magnitude. The evolution of the transverse intensity profile toward its asymptotic state is shown in Fig. 5, and its final configuration is shown in Fig. 6(a). The period of oscillation of the solution, in units of κ^{-1}, is 2.65, which is in excellent agreement with the prediction of Eq. (7.15).

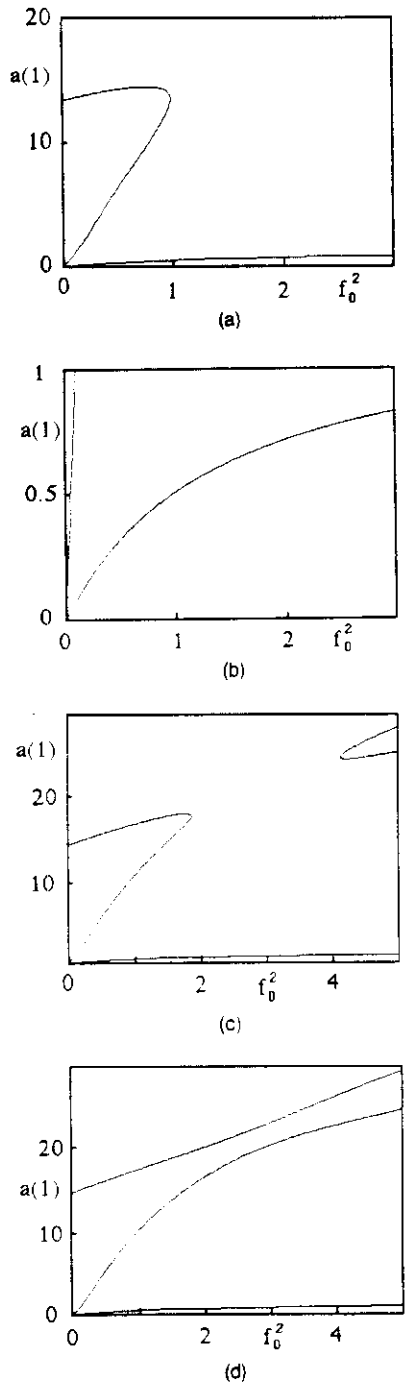

Fig. 3. Instability domain in the plane of the variables $a(1) = a\pi^2$ and f_0^2 for $\kappa' = 0.1$, $\gamma_\parallel/\gamma_\perp = 1$, and (a), (b) $\theta = -0.6$, (c) $\theta = -0.65$, (d) $\theta = -0.67$. (b) Is an expanded version of 3(a) for small values of $a(1)$.

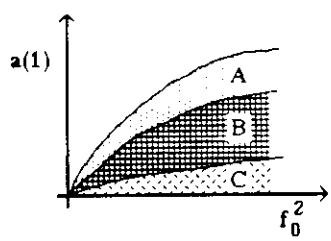

Fig. 4. This figure illustrates qualitatively the regions A, B, and C discussed in the text.

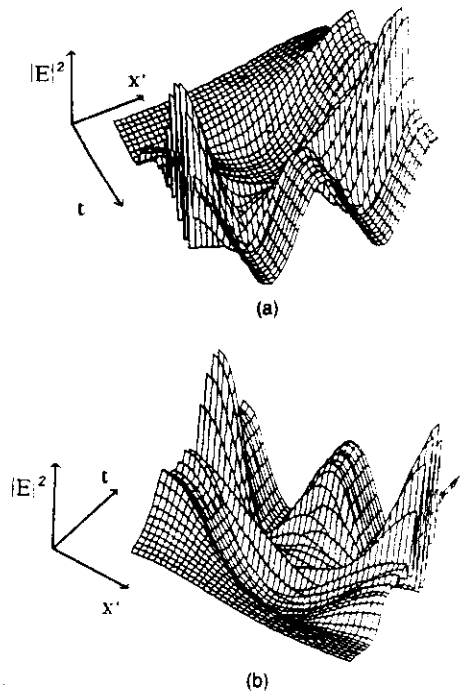

Fig. 5. Time evolution of the transverse intensity profile toward steady state for $\kappa' = 0.1$, $\gamma_\parallel/\gamma_\perp = 1$, $\theta = -0.6$, $f_0^2 = 2$, and $a(1) = 0.65$. (a) and (b) Show the evolution looking backward and forward in time, respectively.

For values of $a(1)$ slightly above region A and following a small initial perturbation around the homogeneous stationary solution (5.7), the system returns to the homogeneous state because of the stable character of the linearized solution. If we begin, instead, with a large initial perturbation, the system approaches a single-mode stationary solution of the type found in region A. This indicates the existence of a hard-mode excitation domain yielding solutions that are direct continuations of those obtained within the unstable domain A.

The value $a(1) = 0.55$ yields a solution in region B. Corresponding to this parameter the system reaches a multimode stationary configuration with the transverse profile shown in Fig. 6(b). After a transient evolution, modes $n = 0$ and $n = 1$ dominate the steady-state picture, as shown in Fig. 7. Here we display the behavior of the aymptotic values of the modal intensity $|f_n|^2$ as a function of $a(1)$ in region B; Fig. 7(a) shows the behavior of $|f_n|^2$ for $n = 0$, 1 and Fig. 7(b) for $n = 2$, 3. Figure 8 displays the variation of the period of oscillation T in units of κ^{-1} over the same interval of $a(1)$. Note that the period seems to diverge as $a(1)$ approaches region C from above. The increase of the period is accompanied also by a marked lengthening of the time required to reach the neighborhood of a stationary solution. When expressed in units of κ^{-1} this time is typically of the order of 100; for $a(1) = 0.2$ (not shown), the time is instead of the order of 800. We interpret this phenomenon as the result of critical slowing down caused by the incipient instability of mode $n = 2$.

For $a(1) = 0.12$, modes $n = 1$ and $n = 2$ are unstable; the system again approaches a multimode stationary state with frequency locking and the transverse intensity profile shown in Fig. 6(c). In this case the odd modes vanish in the long-time limit. Hence this stationary solution is of type (b) with $k = 2$, according to the classification introduced in Section 7,

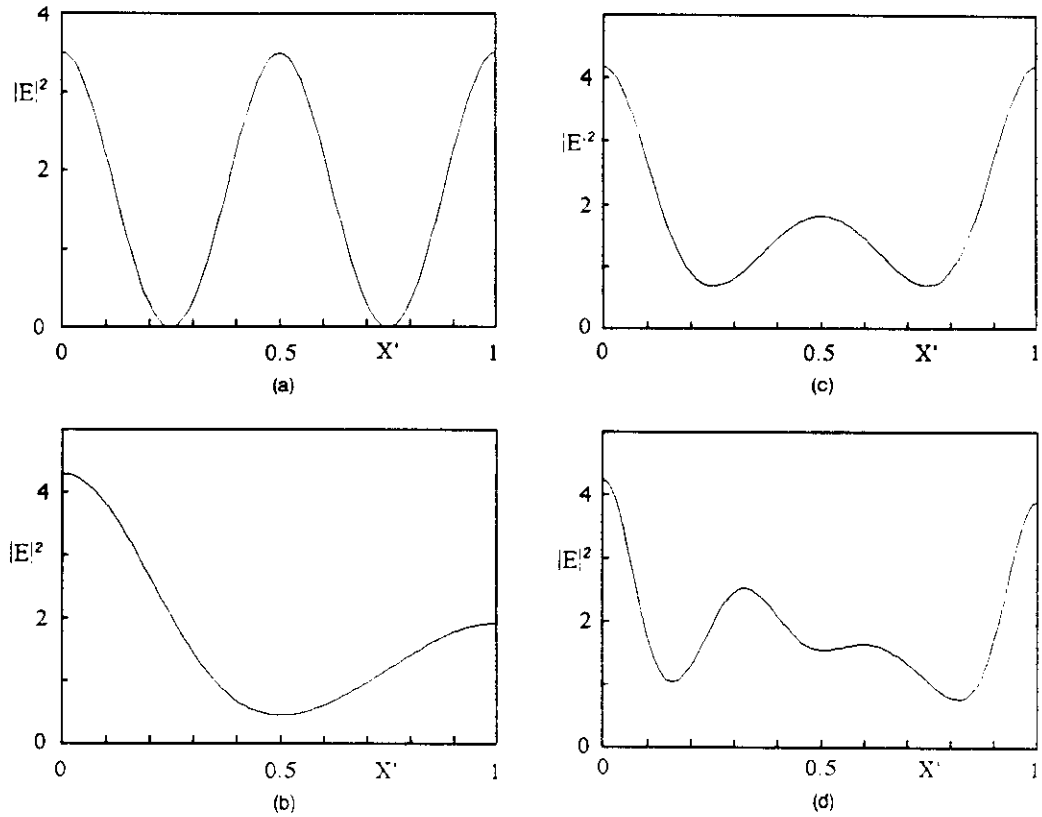

Fig. 6. Transverse profile of the stationary output intensity for $\kappa' = 0.1$, $\gamma_\parallel/\gamma_\perp = 1$, $\theta = -0.6$, $f_0^2 = 2$, and (a) $a(1) = 0.65$, (b) $a(1) = 0.55$, (c) $a(1) = 0.12$, (d) $a(1) = 0.05$.

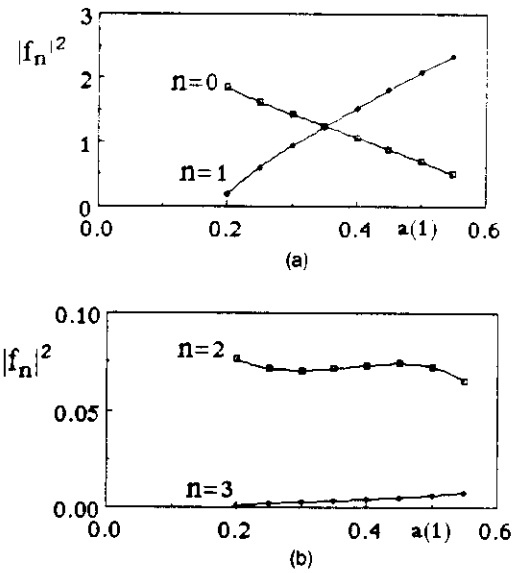

Fig. 7. (a) Plot of the stationary modal intensities for $n = 0$ and $n = 1$ as functions of $a(1)$ over the domain labeled B in Fig. 4. The remaining parameters are the same as in Fig. 6. (b) Is the same as Fig. 7(a) but for modes $n = 2$ and $n = 3$.

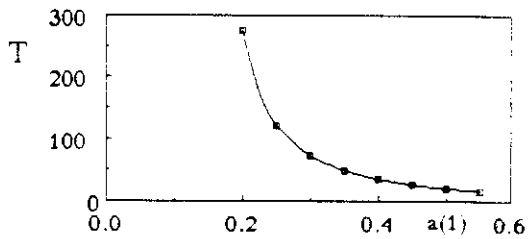

Fig. 8. Behavior of the oscillation period $T = 2\pi/b$ over the same domain of $a(1)$ considered in Fig. 7.

whereas in region B the long-term solution was of type (b) but with $k = 1$. The quantity $|f_2|^2$, in particular, is larger than both $|f_0|^2$ and $|f_4|^2$.

Finally, for $a(1) = 0.05$ the modes $n = 1, 2, 3$ are simultaneously unstable. The long-term solution is a multimode stationary state with odd harmonics that are stronger than their even neighbors [see Fig. 6(d)]. Thus we again have a solution of type (b) with $k = 1$. A fuller description of our numerical analysis will be given in a future publication.

9. CONCLUSIONS AND COMMENTS

In a sense the analysis of this paper is complementary to that of Ref. 15 in spite of the differences between the chosen geometrical configurations (Ref. 15 deals with a traditional ring cavity). These two studies share a common theme: the competition between a longitudinal mode and a set of transverse resonances. The parameters selected in Ref. 15 lead to an intermode spacing for the transverse modes, which is of the order of the cavity free spectral range and, therefore, much larger than the cavity linewidth. As a consequence the resulting instabilities produce spontaneous oscillations of the output intensity instead of stationary spatial patterns.

Our present model, which is based on Eqs. (3.7)–(3.9), predicts both temporal instabilities of the Haken-Lorenz type, which require the bad-cavity condition, $\kappa \gg \gamma_\perp$,[11] and

spatial instabilities that are permitted even in the good-cavity limit. In addition, the eigenvalue equation (6.6) predicts also a large variety of interesting spatiotemporal behaviors for values of κ' that are not necessarily small and that will be analyzed in a subsequent publication.

A class of lasers that comes close to the waveguide configuration considered in this paper should include most semiconductor devices. On the other hand, we can also suggest different types of arrangement. For example, we could eliminate the two lateral mirrors. In this case, we find again the same type of spatial instability involving, now, continuous frequency bands instead of discrete modes [the unstable band is defined by Eq. (6.7)]. This problem is similar to the modulational instabilities described in Ref. 16 for passive systems, but in our case the instability is of the soft-mode type, i.e., it emerges at zero frequency; hence, presumably, it leads again to stationary spatial patterns instead of the dynamical spatiotemporal structures discussed in Ref. 16.

An alternative type of configuration that we could consider in connection with the problem of spatial pattern formation is that of a standard cavity with spherical mirrors. In this case the starting point would coincide with that of Ref. 15 but with a significant difference: the frequency spacing between the radial resonances must be of the order of the cavity linewidth. We may hope that this will lead to the same general picture as illustrated in Section 7. Unfortunately, the spatial structure of the empty cavity modes is governed by Gauss–Laguerre instead of simple trigonometric functions, which is a feature that makes the prospects of analytic progress rather dim. Theoretical efforts along this direction, however, should be encouraged because the standard nature of the cavity geometry with spherical mirror appears significantly more accessible for experimental studies.

APPENDIX A

The coefficients $a_i^{(n)}$ that appear in Eq. (6.6) are given by the following expressions:

$$a_4^{(n)} = 2\gamma_\perp + \gamma_\parallel + 2\kappa, \tag{A1}$$

$$a_3^{(n)} = 2\gamma_\perp\gamma_\parallel + \gamma_\perp\gamma_\parallel f_0^2 + 2\kappa(2\gamma_\perp + \gamma_\parallel) + (\kappa - \gamma_\perp)(1 + \theta^2) + \kappa^2 a(n)[a(n) + 2\theta], \tag{A2}$$

$$a_2^{(n)} = \gamma_\parallel(1 + \theta^2)(\kappa + \gamma_\perp)^2 + \gamma_\perp\gamma_\parallel(\kappa + \gamma_\perp)f_0^2 + 2\kappa\gamma_\perp\gamma_\parallel(2 + f_0^2) + \kappa^2 a(n)(2\gamma_\perp + \gamma_\parallel)[a(n) + 2\theta], \tag{A3}$$

$$a_1^{(n)} = 2\kappa\gamma_\perp\gamma_\parallel(\kappa + \gamma_\perp)f_0^2 + \kappa^2\gamma_\perp a(n)[a(n) \times (2\gamma_\parallel + \gamma_\perp + \theta^2 + \gamma_\parallel f_0^2) + \theta\gamma_\parallel(4 + f_0^2)], \tag{A4}$$

$$a_0^{(n)} = \kappa^2\gamma_\perp^2\gamma_\parallel a(n)[a(n)(1 + \theta^2 + f_0^2) + 2\theta f_0^2]. \tag{A5}$$

where f_0 is defined by Eq. (6.4).

ACKNOWLEDGMENTS

This research was partially supported by a North Atlantic Treaty Organization collaborative research grant and by the European Economic Community twinning project, "Dynamics of Nonlinear Optical Systems." We are grateful to J. R. Tredicce for many useful suggestions and comments and to J. Kohler for assistance with some of the computations. L. M. Narducci wishes to dedicate this work to the memory of Professor Allan E. Parker, spectroscopist, teacher, and friend, whose leadership and affectionate guidance will never be forgotten.

REFERENCES AND NOTES

1. G. Nicolis and I. Prigogine, *Self-Organization in Nonequilibrium Systems* (Wiley, New York, 1977).
2. H. Haken, *Synergetics—An Introduction* (Springer-Verlag, Berlin, 1977).
3. J. D. Murray, J. Theor. Bio. **88**, 161 (1981).
4. A. M. Turing, Phil. Trans. R. Soc. London Ser. B **237**, 37 (1952).
5. N. B. Abraham, L. A. Lugiato, and L. M. Narducci, eds., feature issue on instabilities in active optical media, J. Opt. Soc. Am. B **2**(1) (1985).
6. F. T. Arecchi and R. Harrison, eds., *Instabilities and Chaos in Quantum Optics* (Springer-Verlag, Berlin, 1987).
7. L. A. Lugiato and R. Lefever, Phys. Rev. Lett. **58**, 2209 (1987).
8. L. A. Lugiato, L. M. Narducci, and R. Lefever, in *Lasers and Synergetics—A Volume in Honor of the 60th Birthday of Hermann Haken* (Springer-Verlag, Berlin, 1987).
9. L. A. Lugiato and R. Lefever, in *Interaction of Radiation and Matter, a Volume in Honor of Adriano Gozzini* (Quaderni della Scuola Normale Superiore, Pisa, 1987).
10. L. A. Lugiato and C. Oldano, Phys. Rev. A (to be published).
11. H. Haken, *Light 2—Laser Light Dynamics* (North-Holland, Amsterdam, 1985).
12. H. Zeghlache and P. Mandel, J. Opt. Soc. Am. B **2**, 18 (1985).
13. L. M. Narducci, J. R. Tredicce, L. A. Lugiato, N. B. Abraham, and D. K. Bandy, Phys. Rev. A **33**, 1842 (1986).
14. Here we do not consider the case in which the coefficients f_n have a random relative phase, which produces a stationary output intensity.
15. L. A. Lugiato, F. Prati, D. K. Bandy, L. M. Narducci, P. Ru, and J. R. Tredicce, Opt. Commun. **64**, 167 (1987).
16. D. W. McLaughlin, J. V. Moloney, and A. C. Newell, Phys. Rev. Lett. **54**, 681 (1985).